



Account / Revue

Metal complexes-based molecular materials as thin films on silicon substrates

Dominique de Caro *, Mario Basso-Bert, H el ene Casellas, Mohamed Elgaddari, Jean-Philippe Savy, Jean-Fran ois Lam ere, Alice Bachelier, Christophe Faulmann, Isabelle Malfant, Michel  tienne, Lydie Valade

Laboratoire de chimie de coordination (CNRS UPR 8241), 205, route de Narbonne, 31077 Toulouse cedex 4, France

Received 23 July 2004; accepted after revision 5 November 2004

Available online 26 February 2005

Abstract

A tremendous effort has been devoted in the past two decades to the preparation and study of molecule-based materials derived from organometallic or metalorganic species. The work described in this paper is directed to the study of vapor deposited and electrodeposited thin films of these systems. Amorphous thin films of $M(\text{TCNE})_x$ ($M = \text{V}, \text{Cr}, \text{Nb}, \text{and Mo}$; tetracyanoethylene (TCNE): $(\text{NC})_2\text{C}=\text{C}(\text{CN})_2$) are grown by chemical vapor deposition (CVD) from organometallic complexes and TCNE on (001)-oriented silicon substrates. The films are characterized by infrared spectroscopy, X-ray photoelectron spectroscopy, scanning electron microscopy, and magnetic measurements. Infrared spectra are dominated by CN stretching vibrations and show two main ν_{CN} bands, the positions and relative intensities of which are very similar to those obtained for solution grown $M(\text{TCNE})_{x,y}$ solvent phases (M : first-row transition metal). X-ray photoelectron spectra also confirm the presence of reduced TCNE and low-oxidation state metal atoms in the deposited material. X-ray absorption spectroscopy measurements on $\text{Cr}(\text{TCNE})_x$ films reveal an irregular octahedral environment for the chromium atoms (Cr–N distance of 2.03   and Cr–N–C angle of about 160 ). Magnetic studies show that $M(\text{TCNE})_x$ as thin films are magnetically ordered at low temperatures. Furthermore, after a several hours exposure to air, CVD-grown $\text{V}(\text{TCNE})_x$ films exhibit a spontaneous magnetization at room temperature. Ni(dithiolene)₂-based molecular conductors, namely $[(n\text{-C}_4\text{H}_9)_4\text{N}]_2[\text{Ni}(\text{dcbdt})_2]_5$, and $\text{TTF}[\text{Ni}(\text{dmit})_2]_2$ are electrodeposited on intrinsic silicon wafers used as anodes (dcbdt²⁻: 4,5-dicyanobenzene-1,2-dithiolato; TTF: tetrathiafulvalene; dmit²⁻: 1,3-dithiole-2-thione-4,5-dithiolato). The films are studied by vibrational spectroscopies (Raman and infrared), X-ray photoelectron spectroscopy, X-ray powder diffraction, scanning electron microscopy, and transport measurements. In the former case, the films exhibit a semiconducting behavior with a room temperature conductivity of about $1.2 \times 10^{-2} \text{ S cm}^{-1}$. In the latter case, a metal-like behavior is evidenced in the 14–300 K temperature range. The room temperature conductivity is found to be of ca. 12 S cm^{-1} , which is a non-negligible value, taking into account the presence of numerous inter-grain contacts within the film. **To cite this article:** D. de Caro et al., C. R. Chimie 8 (2005).

  2005 Acad mie des sciences. Published by Elsevier SAS. All rights reserved.

R sum 

Ces vingt derni res ann es, un effort important a  t  consacr    l' laboration et   l' tude des propri t s physico-chimiques de mat riaux mol culaires d riv s de complexes m talliques. Cependant, leur mise en forme, pr alable   toute application poten-

* Corresponding author.

E-mail address: decaro@lcc-toulouse.fr (D. de Caro).

tielle, demeure peu explorée. Ce travail présente deux techniques de mise en forme, le dépôt chimique à partir d'une phase gazeuse et le dépôt électrolytique, qui ont été employées avec succès à la réalisation de films minces de ces systèmes moléculaires. Ces méthodes ont permis la réalisation, d'une part, d'aimants moléculaires du type $M(\text{TCNE})_x$, où M désigne un métal de transition (V, Cr, Nb, Mo) et TCNE le tétracyanoéthylène $(\text{NC})_2\text{C}=\text{C}(\text{CN})_2$, et, d'autre part, de conducteurs moléculaires dérivés de complexes bis(dithiolate) du nickel. Des films minces amorphes des complexes $M(\text{TNCE})_x$ sur substrat de silicium monocristallin de type (001) ont été préparés par dépôt chimique à partir d'une phase gazeuse, en utilisant des complexes organométalliques, sources de l'élément M. Ils ont été caractérisés par spectroscopie infrarouge, spectrométrie de photoélectrons et microscopie électronique à balayage. Le spectre infrarouge est dominé par les vibrations d'élongation ν_{CN} , dont la position et les intensités relatives sont en accord avec l'espèce $\text{TCNE}^{\bullet-}$ coordonnée à plusieurs centres métalliques au nombre d'oxydation +II. La spectrométrie de photoélectrons confirme la présence du tétracyanoéthylène réduit et du métal dans un bas nombre d'oxydation. Le spectre EXAFS enregistré sur le dépôt de $\text{Cr}(\text{TCNE})_x$ révèle un environnement octaédrique distordu autour du chrome. La simulation de ce dernier permet d'extraire les paramètres structuraux suivants : distance Cr–N de 2,03 Å, distance N–C de 1,30 Å et angle Cr–N–C d'environ 160°. Les mesures magnétiques réalisées sur les films de $M(\text{TCNE})_x$ révèlent qu'ils présentent tous une aimantation spontanée à basse température (champ coercitif de 10 à 200 Oe). Le résultat le plus significatif est le caractère de ferri-aimant à température ambiante du dépôt de $\text{V}(\text{TCNE})_x$ même après traitement thermique et exposition à l'air. La méthode de dépôt électrolytique sur anode de silicium a permis l'obtention de films minces cristallins de deux conducteurs moléculaires dérivés de complexes bis(dithiolate) du nickel : d'une part, le composé à nombre d'oxydation fractionnaire $[(n\text{-C}_4\text{H}_9)_4\text{N}]_2[\text{Ni}(\text{dcbdt})_2]_5$ (dcbdt²⁻ : 4,5-dicyanobenzène-1,2-dithiolato), et, d'autre part, le complexe à transfert de charge $\text{TTF}[\text{Ni}(\text{dmit})_2]_2$ (TTF : tetrathiafulvalène ; dmit²⁻ : 1,3-dithiole-2-thione-4,5-dithiolato). Ces dépôts en couche mince ont été caractérisés par les spectroscopies de vibration (infrarouge et Raman), par spectroscopie de photoélectrons, par diffraction des rayons X sur poudre et par microscopie électronique à balayage. Les films minces de $[(n\text{-C}_4\text{H}_9)_4\text{N}]_2[\text{Ni}(\text{dcbdt})_2]_5$ présentent un comportement semiconducteur et une conductivité à température ambiante de $1,2 \times 10^{-2} \text{ S cm}^{-1}$. Les couches minces de $\text{TTF}[\text{Ni}(\text{dmit})_2]_2$ ont un comportement de type métallique. La valeur de la conductivité à température ambiante ($\sim 12 \text{ S cm}^{-1}$) n'est pas négligeable si l'on considère l'inévitable contribution thermo-activée des résistances de contact entre les cristallites. **Pour citer cet article : D. de Caro et al., C. R. Chimie 8 (2005).**

© 2005 Académie des sciences. Published by Elsevier SAS. All rights reserved.

Keywords: Molecular materials; Thin films; Electrodeposition; Chemical vapor deposition; Silicon wafers; Conductivity; Magnetism

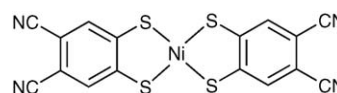
Mots clés : Matériaux moléculaires ; Films minces ; Électrolyse ; Dépôt chimique en phase gazeuse ; Silicium ; Conductivité ; Magnétisme

1. General introduction

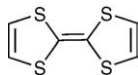
Considerable effort has been recently devoted to the preparation of thin films of organic-based materials [1]. The main techniques used for their preparation are Langmuir–Blodgett, high vacuum evaporation, electrochemical deposition, molecular beam deposition, and chemical vapor deposition (CVD) methods. However, thin films of organometallic- or metalorganic-based materials remain relatively rare. For instance, Prussian blue and Prussian blue-like magnetic materials have been processed as thin films by using either electrodeposition [2–4] or Langmuir–Blodgett [5] techniques. These two methods have also shown their efficiency for growing thin conducting films of bis(dithiolene) complexes [6–8].

In this paper, our goal is to study the processing of metal complexes-based molecular materials on silicon wafers, substrate of choice for electronic applications.

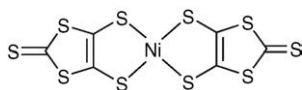
We will illustrate the use of intrinsic silicon (001) wafers in two different processing techniques, i.e. CVD, and electrodeposition. CVD will be applied to prepare thin films of molecule-based magnets of the $M(\text{TCNE})_x$ family (M: V, Cr, Nb, Mo; TCNE: tetracyanoethylene $(\text{NC})_2\text{C}=\text{C}(\text{CN})_2$). Moreover, the electrodeposition technique will be used for processing conducting deposits of $[(n\text{-C}_4\text{H}_9)_4\text{N}]_2[\text{Ni}(\text{dcbdt})_2]_5$ (dcbdt²⁻: 4,5-dicyanobenzene-1,2-dithiolato, Scheme 1) and $\text{TTF}[\text{Ni}(\text{dmit})_2]_2$ (TTF: tetrathiafulvalene, Scheme 2; dmit²⁻: 1,3-dithiole-2-thione-4,5-dithiolato, Scheme 3).



Scheme 1. Molecular structure of $\text{Ni}(\text{dcbdt})_2$.



Scheme 2. Molecular structure of TTF.

Scheme 3. Molecular structure of Ni(dmit)₂.

2. Experimental

2.1. Substrates and starting compounds

Intrinsic Si(001) wafers (one face polished) are purchased from Siltronic (diameter: 5 cm; thickness: 275 μm ; conductivity at room temperature $\sim 10^{-3}$ S cm^{-1}). The wafers are striped in a $\text{NH}_4\text{F}/\text{HF}$ solution (12.5% HF at 50% and 87.5% NH_4F at 40%) and then washed in distilled water before use. TCNE is purchased from Aldrich and freshly sublimed before use. Bis(benzene) vanadium, $\text{V}(\text{C}_6\text{H}_6)_2$, is purchased from Stream Chemicals and bis(benzene) chromium, $\text{Cr}(\text{C}_6\text{H}_6)_2$, is prepared following a previously described procedure [9]. Tris(1,4-diisopropyl-1,4-diazabuta-1,3-diene)niobium, $\text{Nb}(\text{iPr}_2\text{-dad})_3$ [10], and bis(mesitylene)niobium, $\text{Nb}(\text{mes})_2$ [11], are prepared according to the literature data. Bis(toluenemolybdenum), $\text{Mo}(\text{C}_6\text{H}_5\text{CH}_3)_2$, was prepared following a previously described procedure [12]. TTF was purchased from Sigma and used without further purification. $[(n\text{-C}_4\text{H}_9)_4\text{N}][\text{Ni}(\text{dmit})_2]$ was synthesized according to Ref.

[13]. Finally, $[(n\text{-C}_4\text{H}_9)_4\text{N}][\text{Ni}(\text{dcbdt})_2]$ [14] was supplied by Dr. M. Almeida (Departamento de Química, Instituto Tecnológico Nuclear, Sacavém, Portugal).

2.2. CVD procedure

Thin films of $\text{M}(\text{TCNE})_x$ are deposited from TCNE and the metal complex (Table 1), using a conventional hot-wall CVD apparatus [15]. The glass crucibles are charged with the starting compounds inside an argon-filled glove box. The intrinsic Si(001) wafers (1 cm \times 1 cm) are placed on top of a glass slide inside the reactor and the CVD system is then pumped for 15 h down to $\sim 10^{-3}$ Pa, while the carrier lines are heated at 353 K and the reactor at 423 K. The precursors are vaporized at 200 Pa, and transported by helium carrier gas to the mixing zone (448 K) and then to the deposition zone. The mixing zone is held at 448 K in order to avoid condensation of the starting compounds. After their preparation, the films are removed from the deposition zone under an argon flow and finally stored in an argon-filled glove box.

2.3. Electrodeposition procedure

Electrodeposition of $\text{TTF}[\text{Ni}(\text{dmit})_2]_2$ is carried out in a H-shaped electrochemical cell (24 ml) with intrinsic Si(001) as anode (0.5 cm \times 1 cm) and a platinum wire as cathode (solvent: freshly distilled and degassed acetonitrile). We have selected silicon single crystals (vs. polycrystalline silicon) as substrates in order to eliminate spurious effects associated to grain bound-

Table 1
Experimental CVD conditions for film formation of $\text{M}(\text{TCNE})_x$

Precursor mass (mg)	Vaporization temperature (K)	Helium flow rate ($\text{cm}^3 \text{min}^{-1}$)	Substrate zone temperature (K)	Deposition duration (min)
$\text{V}(\text{C}_6\text{H}_6)_2$: 150	418	28	313 (a)	180
TCNE: 180 $\text{Cr}(\text{C}_6\text{H}_6)_2$: 145	356 423	10 17		
TCNE: 190 $\text{Nb}(\text{iPr}_2\text{-dad})_3$: 110	356 418	10 17	353 (b)	90
TCNE: 110 $\text{Mo}(\text{C}_6\text{H}_5\text{CH}_3)_2$: 220	356 388	10 10		
TCNE: 240	356	10	373	40

The deposits are further annealed at (a) 343 K for 10 h, (b) 373 K for 150 min.

Table 2
Experimental conditions for film formation of TTF[Ni(dmit)₂]₂

	Anodic compartment	Cathodic compartment	
TTF (mol)	[(<i>n</i> -C ₄ H ₉) ₄ N][Ni(dmit) ₂] (mol)	[(<i>n</i> -C ₄ H ₉) ₄ N][Ni(dmit) ₂] (mol)	<i>j</i> (μA cm ⁻²)
3.9 × 10 ⁻⁵	1.3 × 10 ⁻⁵	1.3 × 10 ⁻⁵	1.5
6.0 × 10 ⁻⁵	1.0 × 10 ⁻⁵	7.0 × 10 ⁻⁵	0.8
6.0 × 10 ⁻⁵	1.0 × 10 ⁻⁵	7.0 × 10 ⁻⁵	1.5
6.0 × 10 ⁻⁵	1.0 × 10 ⁻⁵	7.0 × 10 ⁻⁵	2.5

Acetonitrile volume in each compartment: 7 ml; 5 days electrolysis.

aries, avoiding e.g. non-homogeneous current densities. The anodic oxidation of the TTF is performed at constant current density at room temperature (Table 2). Within 5 days, a black air-stable thin film is mainly formed on the non-polished face of the (001)-oriented silicon electrode. On the polished face, only a small amount of material is observed but is found to be easily unsticked from the surface due to small mechanical stresses.

Electrodeposition of [(*n*-C₄H₉)₄N]₂[Ni(dcbdt)₂]₅ is carried out on an entire silicon wafer (diameter: 5 cm). A solution of [(*n*-C₄H₉)₄N][Ni(dcbdt)₂] (110 mg) in freshly distilled and degassed CH₂Cl₂ (230 ml) is introduced into a Schlenk-type cylindrical one-compartment electrochemical cell (400 ml). The galvanostatic oxidation (0.5 μA cm⁻²) is performed at 298 K. Within a day, black microcrystals appear and grow homogeneously on the Si surface. A ~10 μm continuous, adherent and air-stable thin film is obtained after a 4 days electrolysis duration.

2.4. Characterization methods

Scanning electron micrographs (SEM) are obtained on a JEOL Model JSM 840A microscope. Infrared spectra are recorded using a Perkin–Elmer Spectrum GX spectrophotometer. The Raman measurements are performed using a DILOR XY micro-Raman set-up. The spectra are obtained at room temperature using the 647 nm line of a Kr laser. The incident beam is focused onto the film through the × 100 microscope objective, giving a spot size of ~1 μm². The back-scattered light is collected through the same objective, dispersed and then imaged onto a CCD detector. Using a laser power density of about 10⁵ W cm⁻², no major degradation of the material appears. X-ray diffraction data are collected with a Seifert XRD 3000 TT, using the Cu Kα radiation (1.5418 Å), fitted with a diffracted beam monochromator. The diffractometer is in Bragg–Bren-

tano configuration (θ/θ). XPS spectra of magnetic thin films are recorded using a VG Escalab Model MK2 spectrophotometer, working with monochromatic Mg Kα radiation (1253.6 eV). X-ray photoelectron spectra of conducting thin films are acquired with an EA10P hemispherical analyzer (SPECS) using non-monochromatized Al Kα radiation (1486.6 eV). X-ray absorption spectra of Cr(TCNE)_x deposits are performed on the XAS 13 beam line at the French synchrotron facility DCI at LURE (Orsay). Spectra are recorded at the chromium K-edge in transmission mode using Si 311 (X-ray absorption near edge structure, XANES) and Si 111 (extended X-ray absorption fine structure, EXAFS) double monochromator detuned around 30% to ensure harmonic rejection. The edge energy of the chromium (5989 eV) is fixed at the first inflexion point of a chromium foil. Magnetic data are taken on a MPMS 5.5 Quantum Design SQUID magnetometer. Conductivity measurements are performed using the standard four-probe method. Electrical contacts between the gold wires and the film are made by using gold paint. They are drawn parallel to each other keeping a large inter-wire distance (~2.2 mm).

3. Results and discussion

3.1. M(TCNE)_x magnets as thin films

3.1.1. Introduction

Recently, the study of molecule-based magnets exhibiting spontaneous magnetization at room temperature has attracted increasing interest [16,17]. These light weight materials, obtained from an organometallic route, represent an interesting alternative to conventional magnets in future generations of devices. M(TCNE)_x, *y* solvent ($x \sim 2$; $0.5 \leq y \leq 2$; M: first-row transition metal, namely, V, Mn, Fe, Co, Ni) are molecule-based ferrimagnets with critical temperatures ranging

from 45 to 400 K and coercive fields as great as 6.5 kOe [18]. We have recently reported the preparation of $M(\text{TCNE})_x$ (M : V, Cr) magnets as thin films on alkali halide substrates using CVD [19,20]. However, alkali halides are not the most appropriate for potential applications. Moreover, deposits obtained on alkali halides were found to be easily unsticked due to small mechanical stresses. On the other hand, it is to be noticed that $M(\text{TCNE})_x$, γ solvent systems are not known with second-row transition metals. In the following 3.1.2 and 3.1.3 paragraphs, we describe the use of CVD to the formation of solvent free- $M(\text{TCNE})_x$ (M : V, Cr, Nb, Mo) molecular magnets on silicon, this latter constituting a more suitable substrate for potential applications.

3.1.2. Vanadium and chromium-based magnets

Thin films of the $V(\text{TCNE})_x$ phase are deposited on silicon substrates from $V(\text{C}_6\text{H}_6)_2$ and TCNE, in the conditions reported in Table 1. The loss of the benzene rings occurs at a relatively low temperature (313 K). The black deposits thus obtained have an amorphous character. The films do not spontaneously peel off (contrary to what observed on alkali halides). However, the deposits are very sensitive towards air exposure. To improve their stability (~ 1 h), they are further annealed at 343 K for 10 h under a helium atmosphere. After the thermal treatment, the amorphous character of the films is maintained. SEM images of annealed films evidence roughly spherical sub-micrometer grains (Fig. 1). The infrared spectra show no ν_{CH} bands corresponding to the presence of the aromatic ligands, thus confirming the loss of the benzene rings. Furthermore, two broad ν_{CN} bands are observed at 2106(s) and 2195(m) cm^{-1} (Fig. 2), consistent with a monoreduced TCNE moiety

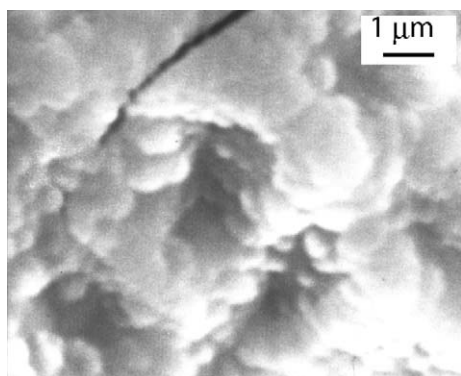


Fig. 1. SEM image of annealed $V(\text{TCNE})_x$ thin films.

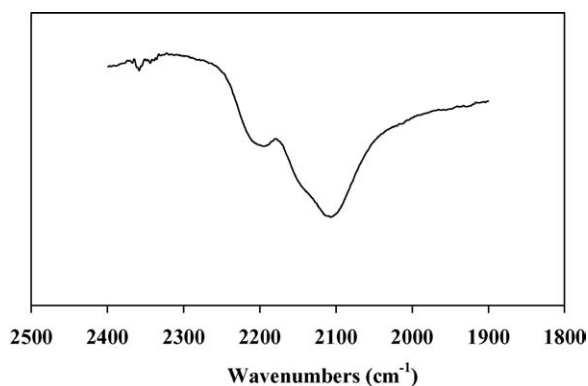


Fig. 2. IR spectrum of annealed $V(\text{TCNE})_x$ thin films (ν_{CN} region).

($\text{TCNE}^{\bullet-}$) bound to four vanadium atoms via σ -N bonds [18]. A shoulder at 2145 cm^{-1} is also observed and may be assigned to $\text{TCNE}^{\bullet-}$ *trans*- μ -bound to two vanadiums [21]. X-ray photoelectron data evidence the presence of V, C, N and O. The presence of oxygen (< 1 at.%) is due to surface contamination. The N1s peak is at 397.7 eV, in agreement with monoreduced TCNE, i.e. $\text{TCNE}^{\bullet-}$ [22]. The $V2p_{3/2}$ line has a binding energy at 513.3 eV, a typical value for V^{II} [23]. The magnetization measurements at 5 K for the annealed films reveal a saturation magnetization of ~ 0.5 emuOe g^{-1} . This value is lower than that observed for as-deposited $V(\text{TCNE})_x$ films (~ 18 emuOe g^{-1} , Fig. 3). J.S. Miller et al. also reported that thermal treatment of solution grown $V(\text{TCNE})_2 \cdot 0.5\text{CH}_2\text{Cl}_2$ reduced the magnetization values [18]. It is to be remarked that as-deposited $V(\text{TCNE})_x$ shows only two broad ν_{CN} absorptions at 2105(s) and 2192(m) cm^{-1} , attributable to $\text{TCNE}^{\bullet-}$ bound to four vanadiums [19]. For the annealed films, some $\text{TCNE}^{\bullet-}$ s seems to be *trans*- μ -bound to two vanadiums (further absorption at 2145 cm^{-1}). This partial decoordination from the V^{II} centers would block some spin-

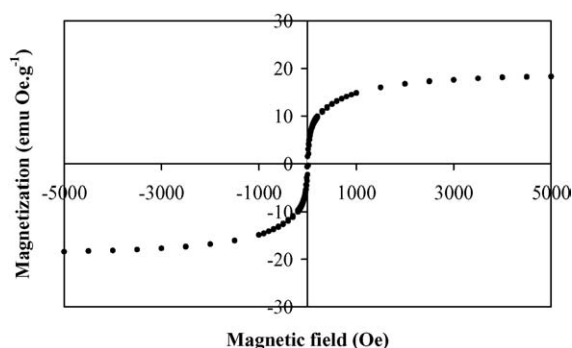


Fig. 3. Hysteresis loop at 5 K for as-deposited $V(\text{TCNE})_x$ thin films.

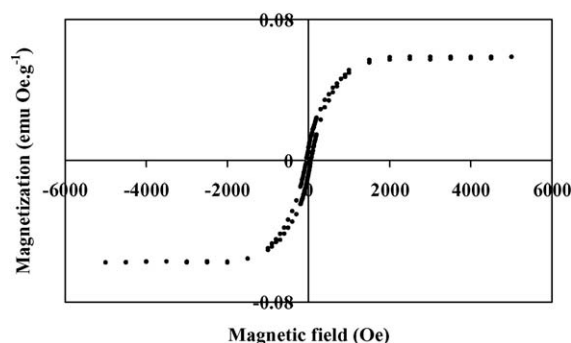


Fig. 4. Hysteresis loop at 300 K for annealed $V(TCNE)_x$ thin films.

coupling pathways and could induce magnetic disorder. However, after thermal treatment, a spontaneous magnetization remains at room temperature as shown on Fig. 4. The hysteresis loop (magnetization vs. applied magnetic field) evidences a coercive field of ~ 50 Oe and a saturation induction of ~ 2.5 kOe, to be compared to ~ 80 Oe and ~ 0.8 kOe for as-deposited $V(TCNE)_x$ [19]. Furthermore, after thermal treatment and air exposure (Fig. 5), a hysteresis loop is still observed at room temperature (coercive field ~ 50 Oe and saturation magnetization $\sim 1.2 \times 10^{-2}$ emuOe g^{-1} , to be compared to ~ 50 Oe and $\sim 5.9 \times 10^{-2}$ emuOe g^{-1} for annealed samples without air exposure).

Black amorphous thin films of $Cr(TCNE)_x$ are prepared on silicon substrates via CVD of $Cr(C_6H_6)_2$ and TCNE precursors (Table 1). The loss of the benzene rings is achieved when operating at 353 K and further annealing the deposits at 373 K for 2 h under a helium flow. As observed for the vanadium-based deposits, $Cr(TCNE)_x$ as thin films do not spontaneously peel off from the silicon surface. The films can be handled in air for ~ 5 h. SEM micrographs evidence a uniform film in which numerous cracks are clearly observed (Fig. 6).

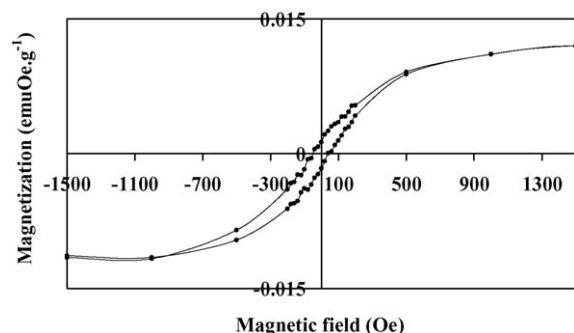


Fig. 5. Hysteresis loop at 300 K for annealed $V(TCNE)_x$ thin films after air exposure.

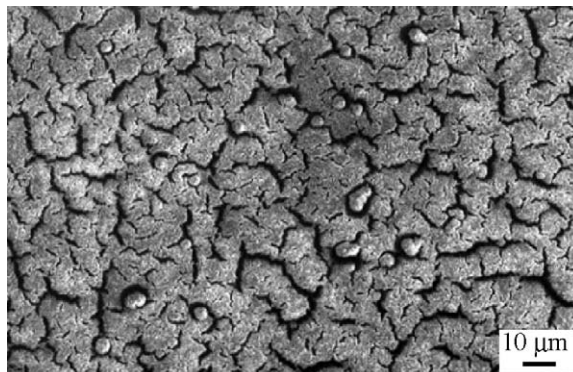


Fig. 6. SEM image of $Cr(TCNE)_x$ thin films.

However, their presence does not affect too much the adherence of the films onto the Si surface. The infrared spectra show two broad ν_{CN} bands at 2116(s) and 2202(m) cm^{-1} , consistent with $TCNE^{\bullet-}$ ligands coordinated as $\mu_n-N-\sigma$ to the metal ($n = 2-4$) [16]. The $Cr2p_{3/2}$ line has a binding energy at 576.3 eV, a typical value for Cr^{II} organometallic complexes, such as $Cr(C_5H_5)_2$ [24]. The chromium K-edge spectrum (XANES) of $Cr(TCNE)_x$ is shown on Fig. 7. Its overall feature is in agreement with that of octahedral $[ML_6]^{2+}$ complexes ($M = V^{II}$ to Cu^{II}) [25]. The top of the edge energy is 6009 eV (C), close to that for low-oxidation state chromium (Cr^{II} or Cr^{III}). The D signal is due to multiple scattering [25]. The spectrum also displays two peaks of weak intensity at 5992 eV (A) and 5996 eV (B). Signal A is assigned to 1s to 3d transitions, forbidden in regular octahedral complexes, but partially allowed in irregular ones [26]. The presence of this peak evidences an irregular octahedral environment for the chromium atoms within the deposit. Signal B is assigned to an allowed transition from 1s to a molecular orbital combining p orbitals of the chromium and π^*_{CN}

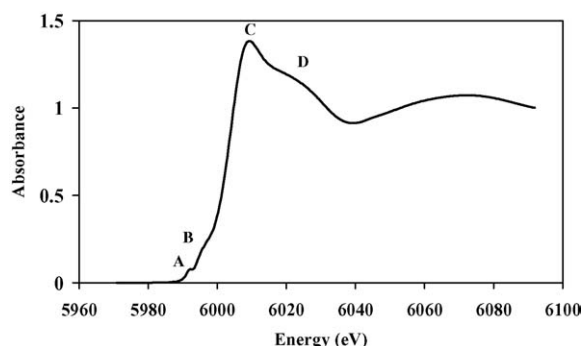


Fig. 7. XANES chromium K-edge spectrum of $Cr(TCNE)_x$ thin films.

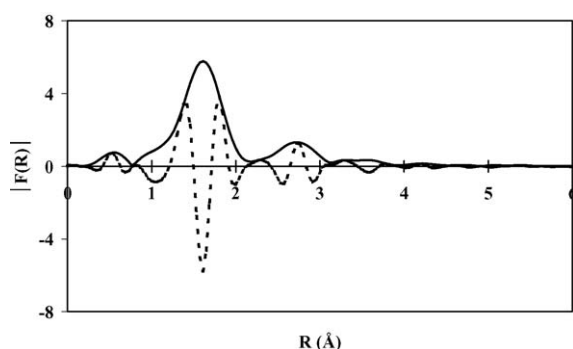


Fig. 8. Fourier transform modulus $|F(R)|$ (solid line) and imaginary part (dotted line) of the EXAFS signal at the chromium K-edge.

[26], thus confirming the presence of coordinated $\text{TCNE}^{\bullet-}$. At the chromium K-edge, the Fourier transform of the EXAFS signal displays two peaks assigned to two shells around the chromium (Fig. 8). They correspond to the nitrogen and carbon atoms of the TCNE ligand. To extract information about the distances and the bond angles around the metallic atoms, we model the EXAFS signal using the FEFF7 code [27]. The structural parameters that fit best with the experimental data are the following: six nitrogen neighbors around chromium, a mean Cr–N distance of 2.03 Å, a N–C distance of 1.30 Å and a 160° Cr–N–C angle. It is to be remarked that the Cr–N distance in cyanato ($\text{N}=\text{C}=\text{O}$), thiocyanato ($\text{N}=\text{C}=\text{S}$) and alkylideneamido ($\text{N}=\text{CRR}$) Cr^{III} -complexes are in the range 1.95–1.99 Å [28]. In our case, a larger Cr–N distance suggests a lower oxidation state, i.e. Cr^{II} , thus confirming XPS results. The 2–300 K magnetic susceptibility of the films can be fit to the Curie–Weiss law above 80 K with a θ value of -95 K (Fig. 9). Consequently, the magnetic interaction between the spin centers is strongly antiferromagnetic. At 2.5 K, the magnetization value for an applied field

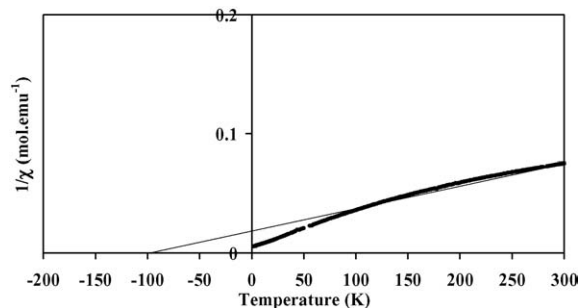


Fig. 9. Reciprocal magnetic susceptibility vs. temperature for $\text{Cr}(\text{TCNE})_x$ thin films.

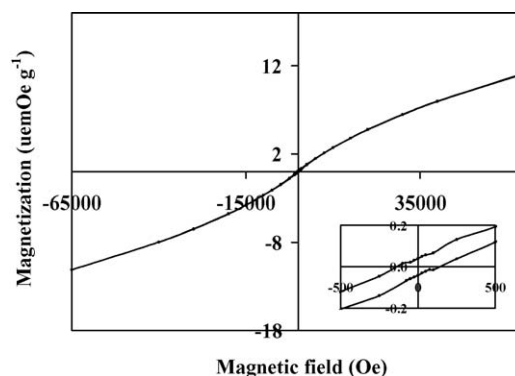


Fig. 10. Hysteresis loop at 2.5 K for $\text{Cr}(\text{TCNE})_x$ thin films.

of 65 kOe is ~ 11 $\mu\text{emOe g}^{-1}$ (Fig. 10). Inset in Fig. 10 shows the hysteresis loop recorded in the low-field region at 2.5 K (coercive field ~ 100 Oe). It clearly evidences that the films exhibit spontaneous magnetization at this temperature, whilst the corresponding $\text{Cr}(\text{TCNE})_{x,y}$ solvent are not magnetically ordered above 2 K, presumably due to the deleterious effect of the solvent molecules [29].

3.1.3. Niobium and molybdenum-based magnets

Black amorphous thin films of $\text{Nb}(\text{TCNE})_x$ are grown from the gas phase reaction of $\text{Nb}(\text{iPr}_2\text{-dad})_3$ and TCNE. They are air sensitive but relatively adherent on Si(001) wafers. The infrared spectrum of the films exhibits three bands at 2200(s), 2180(sh), and 2102(s) cm^{-1} (Fig. 11). They are in agreement with the presence of reduced TCNE moieties bound to Nb. The N1s X-ray photoelectron spectrum has two components at 398.1 and 399.9 eV, respectively, assigned to nitrogen atoms in $\text{TCNE}^{\bullet-}$ bound to Nb and to nitrogen atoms in TCNE^0 , the oxidation product of $\text{TCNE}^{\bullet-}$ [22].

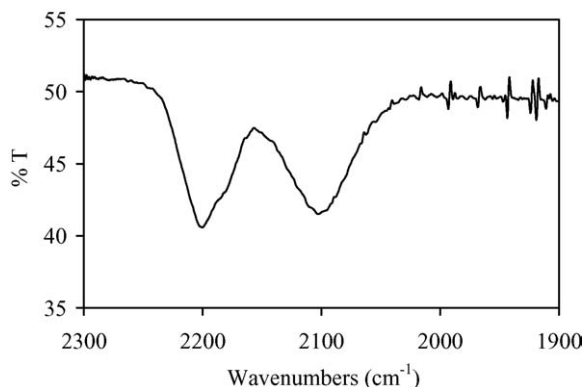


Fig. 11. IR spectrum of $\text{Nb}(\text{TCNE})_x$ thin films (ν_{CN} region).

XPS analyses also evidence that the Nb3d_{5/2} and Nb3d_{3/2} lines are split into two components at 204.4, 206.3, 207.2, and 209.2 eV. The 204.4 and 207.2 peaks (60%) are attributed to Nb^{II} by comparison with XPS data related to Nb²⁺ ions implanted into sapphire [30]. The other peaks (40%) correspond to NbO₂ [31], whose presence is assigned to surface oxidation caused by handling the samples in the air before XPS measurements. After a bombardment of the films by Ar⁺ ions for 15 min. which allows the removal of the surface oxide, the XPS spectrum shows then clearly two peaks (6:4) corresponding to the 3d_{5/2} (204.6 eV) and 3d_{3/2} (207.4 eV) levels of Nb^{II}. SEM images evidence a film uniformly covering the substrate surface (Fig. 12). Some defects occasionally encountered allow us to evaluate the thickness of the film at ~3 μm. Magnetic measurements evidence that the films exhibit a spontaneous magnetization at 2.5 K. Fig. 13 shows the first and the second magnetization curves at this tempera-

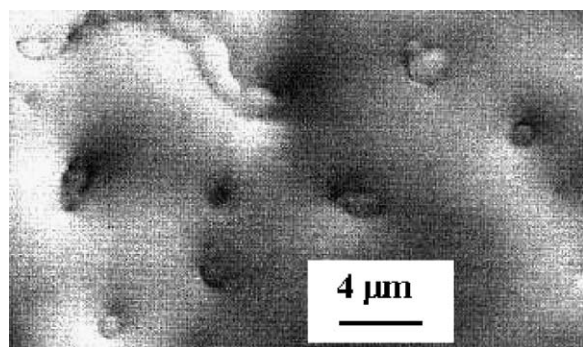


Fig. 12. SEM image of Nb(TCNE)_x thin films.

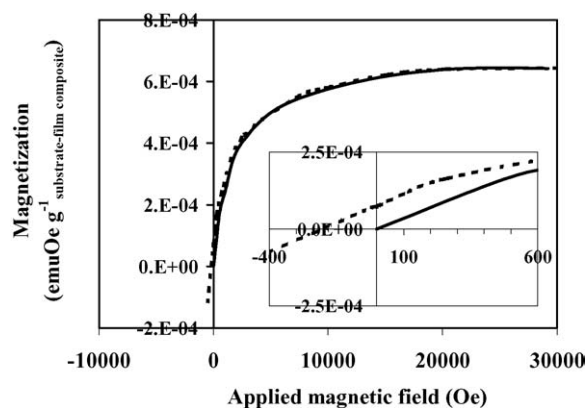


Fig. 13. Magnetization vs. applied magnetic field for Nb(TCNE)_x thin films at 2.5 K (first magnetization: solid line, second magnetization: dotted line).

ture. They evidence a saturation induction of ~20 kOe and a coercive field of ~200 Oe.

Black amorphous thin films of Mo(TCNE)_x are prepared via CVD of Mo(C₆H₅CH₃)₂ and TCNE precursors. They are very adherent on Si(001) wafers. X-ray photoelectron spectra show the presence of Mo, C, N, and O. The presence of oxygen (0.3 at.%) is assigned to surface contamination. The N/Mo atomic ratio is found to be 7.3, a value in rather good agreement with a 1 Mo/2 TCNE stoichiometry (MoC₁₂N₈). The Mo3d_{5/2} and Mo3d_{3/2} lines are located at 228.7 and 231.8 eV, respectively (areas ratio: 1.33, in reasonable agreement with the theoretical value of 6/4). The Mo3d_{5/2} has a binding energy very close to that for Mo^{II} complexes, such as Mo(C₅H₅)(CO)₃Cl (228.7 eV) and Mo(C₅H₅)(CO)₃[Sn(CH₃)₃] (228.5 eV) [32]. The N1s signal (399.2 eV) has a binding energy consistent with the presence of TCNE^{•-}. This value is in good agreement with that obtained for [Mn^{III}(TPP)][TCNE], 2 C₆H₅CH₃ (TPP = *meso*-tetraphenylporphyrin), i.e. 399.1 eV (*trans*-μ-TCNE^{•-} moiety) [33]. Infrared spectra show two ν_{CN} broad bands at 2212(s) and 2113(m) cm⁻¹ (Fig. 14), close to those observed for [Mn(C₅Me₅)(CO)₂][TCNE] (2205 and 2125 cm⁻¹) in which TCNE is *trans*-μ-N-bound to manganese(II) [34]. Moreover, no ν_{CH} bands (3070–2800 cm⁻¹ region) corresponding to the presence of toluene rings are observed. SEM images (Fig. 15) evidence a cracked film on which roughly spherical agglomerated grains are randomly dispersed (average size of the spherical grains: 1.5 μm). Fig. 16 shows the hysteresis loop (magnetization vs. applied magnetic field) at 2 K. The sample nearly saturates for an applied magnetic field of 50 kOe and a coercive field of ~20 Oe is observed.

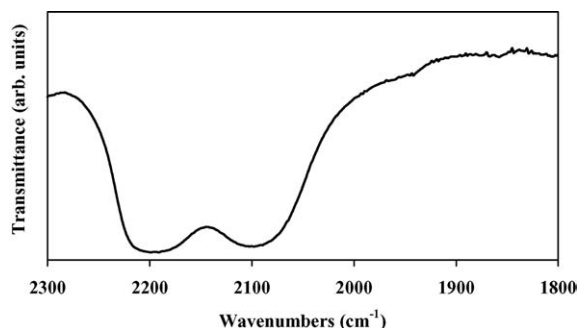
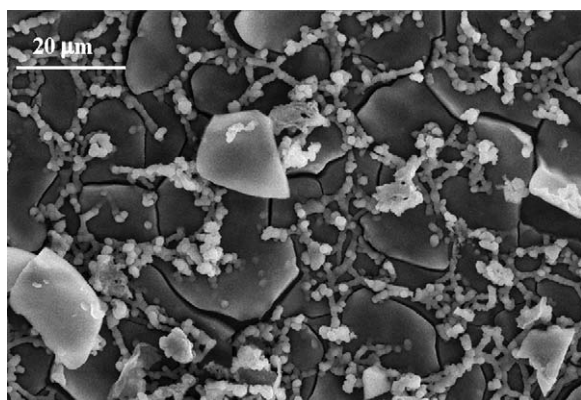
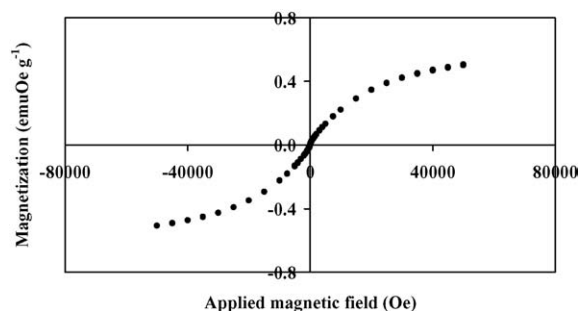


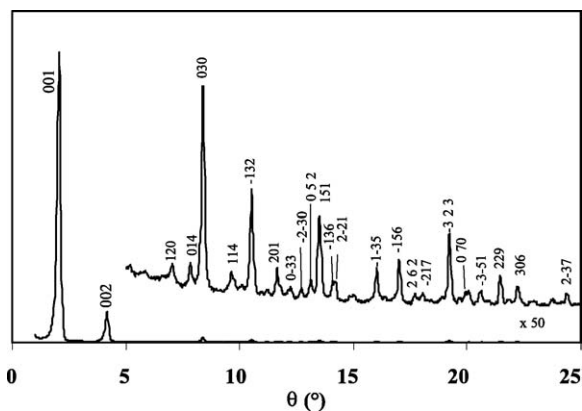
Fig. 14. IR spectrum of Mo(TCNE)_x thin films (ν_{CN} region).

Fig. 15. SEM image of Mo(TCNE)_x thin films.Fig. 16. Hysteresis loop at 2 K for Mo(TCNE)_x thin films.

3.2. Conductors based on bis(dithiolene) complexes as thin films

3.2.1. Introduction

Homoleptic dithiolene complexes $M L_2$ (L: 1,1-, 1,2- or 1,3-dithiolene ligand) have been extensively considered as a key unit to build up molecule-based materials exhibiting a metallic behavior [35]. To obtain a metallic state, partial filling of the conduction band is required. This may be obtained either through partial oxidation, as in non-integral oxidation state salts, or through partial charge transfer, as in donor–acceptor adducts. The $(\text{cation})_x[M(\text{dithiolene})_2]$ salts are prepared either by chemical or electrochemical oxidation of the appropriate $(\text{cation})[M(\text{dithiolene})_2]$ salt. The $D[M(\text{dithiolene})_2]_y$ (D: donor molecule) compounds can be prepared either by electrochemical oxidation of the donor molecule in the presence of the appropriate $(\text{cation})[M(\text{dithiolene})_2]$ salt or by metathesis reaction between the appropriate D(anion) and $(\text{cation})[M(\text{dithiolene})_2]$ salts.

Fig. 17. X-ray diffraction pattern for electrodeposited $[(n\text{-C}_4\text{H}_9)_4\text{N}]_2[\text{Ni}(\text{dcbdt})_2]_5$ thin films.

We present in the following 3.2.2 and 3.2.3 paragraphs, the preparation of electrodeposited thin films of two Ni(dithiolene)₂-based conductors, namely the non-integral oxidation state salt $[(n\text{-C}_4\text{H}_9)_4\text{N}]_2[\text{Ni}(\text{dcbdt})_2]_5$ (dcbdt^{2-} : 4,5-dicyanobenzene-1,2-dithiolato), and the donor–acceptor adduct $\text{TTF}[\text{Ni}(\text{dmit})_2]_2$ (TTF: tetrathiafulvalene; dmit^{2-} : 1,3-dithiole-2-thione-4,5-dithiolato).

3.2.2. Electrodeposited films of $[(n\text{-C}_4\text{H}_9)_4\text{N}]_2[\text{Ni}(\text{dcbdt})_2]_5$

$[(n\text{-C}_4\text{H}_9)_4\text{N}]_2[M(\text{dcbdt})_2]_5$ (M = Ni, Au) single crystals can be prepared as thin plates ($3 \times 0.3 \times 0.05 \text{ mm}^3$) on the surface of a platinum anode, by electrocrystallization from the corresponding $[(n\text{-C}_4\text{H}_9)_4\text{N}][M(\text{dcbdt})_2]$ complex under galvanostatic conditions [14,36]. Both compounds present a triclinic structure (*P*-1) showing stacks of pentamerized $M(\text{dcbdt})_2$ units along $[-210]$. The electrical conductivity measured along the long axis $[-210]$ of the elongated-shaped crystals denotes a semi-conducting behavior ($\sigma_{\text{RT}} = 0.13 \text{ S cm}^{-1}$ and activation energy $E_a = 0.176 \text{ eV}$ for M = Ni; $\sigma_{\text{RT}} = 10 \text{ S cm}^{-1}$ and $E_a = 0.027 \text{ eV}$ for M = Au).

Thin films of $[(n\text{-C}_4\text{H}_9)_4\text{N}]_2[\text{Ni}(\text{dcbdt})_2]_5$ are obtained by galvanostatic electrolysis on a silicon wafer in a one-compartment cell containing a dichloromethane solution of $[(n\text{-C}_4\text{H}_9)_4\text{N}][\text{Ni}(\text{dcbdt})_2]$. The films uniformly cover the substrate surface. X-ray powder diffraction data evidence a highly oriented film (Fig. 17). Refinement of the collected data gives the following crystallographic parameters: $a = 7.999(8) \text{ \AA}$, $b = 17.271(2) \text{ \AA}$, $c = 22.490(3) \text{ \AA}$, $\alpha = 69.01(1)$, $\beta = 89.08(1)$, $\gamma = 78.90(1)$, to be compared with

$a = 8.000(1) \text{ \AA}$, $b = 17.288(3) \text{ \AA}$, $c = 22.490(4) \text{ \AA}$, $\alpha = 69.181(8)$, $\beta = 89.161(12)$, $\gamma = 78.14(1)$ obtained from single crystal study [37]. The very good agreement of the lattice parameters confirms the 2:5 stoichiometry and shows that the deposition process does not affect the structural arrangement of the compound although the very weak intensity of the diffraction lines other than (001) and (002) may limit the precision of the measurement. The growth of the film is then found to be highly anisotropic, the ab -plane being parallel to the wafer surface. Electron micrographs evidence that the film is made of thin platelets (30–55 μm long, 1–8 μm width, thickness $< 1 \mu\text{m}$) randomly distributed on the substrate surface (Fig. 18a). Moreover, a SEM side view of a segment of the film peeled off from the surface allows us to evaluate the thickness at $\sim 10 \mu\text{m}$. Raman spectra performed on the film (Fig. 19a) and on the precursor material (Fig. 19b) exhibit almost the same characteristic vibrational bands. Bands at 405(m),

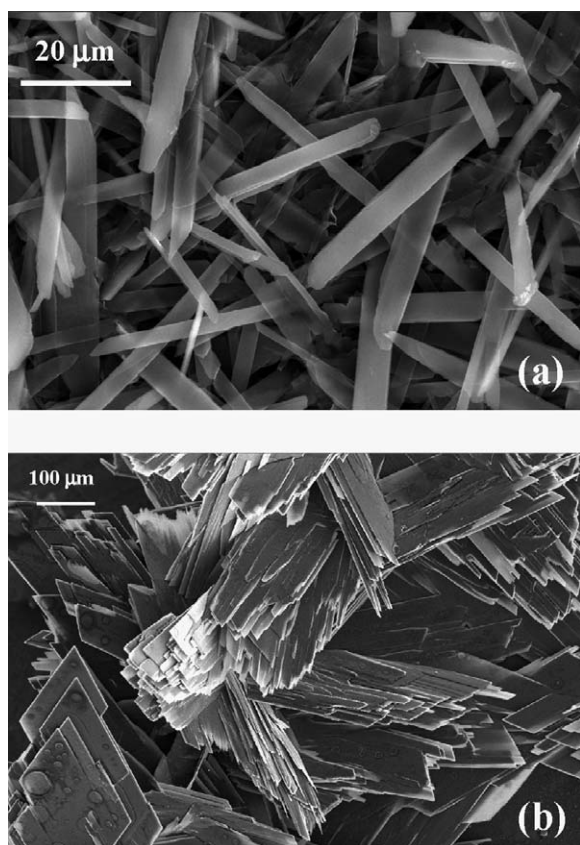


Fig. 18. SEM images of deposits of $[(n\text{-C}_4\text{H}_9)_4\text{N}]_2[\text{Ni}(\text{dcbdt})_2]_5$ under galvanostatic conditions (a), potentiostatic conditions (b).

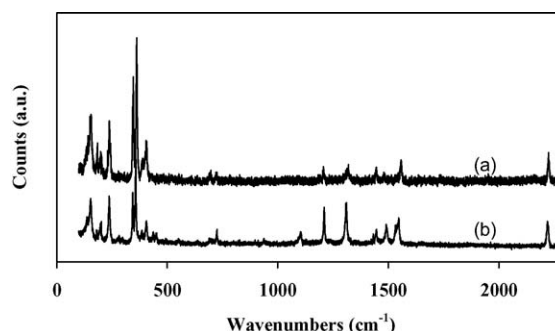


Fig. 19. Raman spectra of deposits of $[(n\text{-C}_4\text{H}_9)_4\text{N}]_2[\text{Ni}(\text{dcbdt})_2]_5$ (a) and of the starting $[(n\text{-C}_4\text{H}_9)_4\text{N}][\text{Ni}(\text{dcbdt})_2]$ complex (b).

362(s) and 347(s) cm^{-1} are, respectively, assigned to C–S stretching, Ni–S stretching, and out of phase deformation of the five-membered rings connected to the nickel [38,39]. It should be noted that medium intensity Raman signals appearing at 1546 cm^{-1} (aromatic C=C stretching modes) and 2220 cm^{-1} (CN stretching modes) for the precursor compound shift to higher frequencies, that is 1557 and 2225 cm^{-1} , respectively, for the film. This frequency shift is in agreement with the decrease of the average value of the charge of the Ni(dcbdt)₂ moiety $[\text{Ni}(\text{dcbdt})_2]^- \rightarrow \text{Ni}(\text{dcbdt})_2^{0.4-}$, as previously reported in the case of thin films of $[(n\text{-C}_4\text{H}_9)_4\text{N}]_{0.9}[\text{Ni}(\text{dmid})_2]$ [7]. From the infrared spectrum, we see that, also due to the charge change of the complex in the deposit relatively to $[\text{Ni}(\text{dcbdt})_2]^-$, carbon–hydrogen stretching vibrations of the phenyl groups are shifted from 3061 cm^{-1} in the starting complex to 3067 cm^{-1} in the film (Fig. 20). As expected, CH stretching modes of butyl groups of the $[(n\text{-C}_4\text{H}_9)_4\text{N}]^+$ cations (2850–2965 cm^{-1}) remain unchanged after partial oxidation of $[(n\text{-C}_4\text{H}_9)_4\text{N}][\text{Ni}(\text{dcbdt})_2]$. The nitrile vibration modes are present at 2226 cm^{-1} in the infrared spectrum of the deposit, a

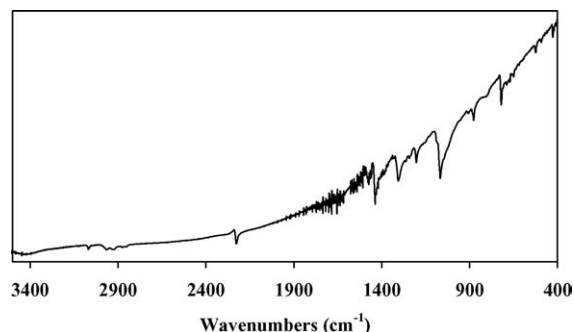


Fig. 20. Infrared spectrum of deposits of $[(n\text{-C}_4\text{H}_9)_4\text{N}]_2[\text{Ni}(\text{dcbdt})_2]_5$.

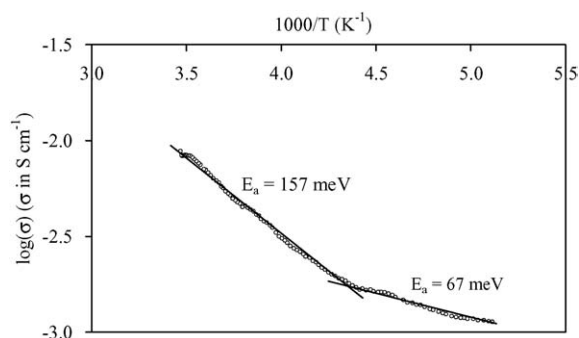


Fig. 21. Conductivity as a function of reciprocal temperature for electrodeposited $[(n\text{-C}_4\text{H}_9)_4\text{N}]_2[\text{Ni}(\text{dcbdt})_2]_5$.

value almost identical to that observed in the Raman spectrum. The electrical conductivity of $[(n\text{-C}_4\text{H}_9)_4\text{N}]_2[\text{Ni}(\text{dcbdt})_2]_5$ thin films is about $1.2 \times 10^{-2} \text{ S cm}^{-1}$ at room temperature and follows a thermally activated semiconducting behavior. The plot of $\log(\sigma)$ versus $1/T$ shows an activation energy of 157 meV in the range 295–230 K (Fig. 21). This value is reduced to 67 meV below 230 K.

3.2.3. Electrodeposited films of $\text{TTF}[\text{Ni}(\text{dmit})_2]_2$

$\text{TTF}[\text{Ni}(\text{dmit})_2]_2$ belongs to the donor–acceptor family of compounds. Within the final material, the charge transfer between the TTF donor molecule and the $[\text{Ni}(\text{dmit})_2]$ acceptor complex was found to be 0.8 from diffuse X-ray scattering experiments and band structure calculations [40]. The structure of $\text{TTF}[\text{Ni}(\text{dmit})_2]_2$ consists of segregated stacks of TTF and $[\text{Ni}(\text{dmit})_2]$ units. On single crystal, its room-temperature conductivity is $\sim 300 \text{ S cm}^{-1}$ at ambient pressure along [010]. The conductivity behavior is metallic down to 4 K. Moreover, this compound undergoes a complete transition to a superconducting state at 1.62 K under a hydrostatic pressure of 7 kbar [41].

Electrodeposition of $\text{TTF}[\text{Ni}(\text{dmit})_2]_2$ is carried out with intrinsic Si(001) as anode and a platinum wire as cathode in an H-shaped electrochemical cell (Table 2). XPS data confirm the 1 TTF/2 $[\text{Ni}(\text{dmit})_2]$ stoichiometry for the films. Fig. 22 shows the XPS S2p line measured on $\text{TTF}[\text{Ni}(\text{dmit})_2]_2$ thin films. The experimental lineshape can be satisfactorily decomposed in three contributions. The most intense line, with a binding energy of 163.5 eV, corresponds to C–S–C, as already reported for TTF derivatives [42]. We assign the 161.8 and 165.3 eV lines to C–S–Ni and C=S, respectively, based

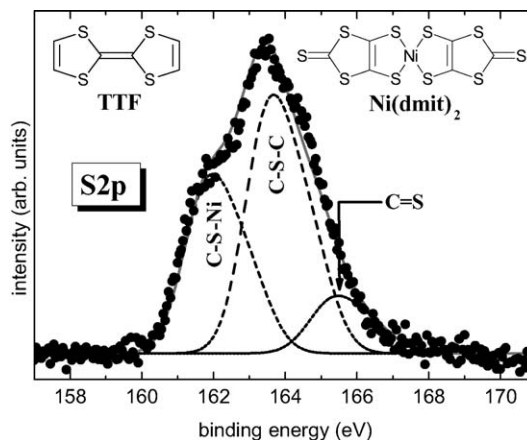


Fig. 22. XPS S2p line (black dots) measured at room temperature of a $\text{TTF}[\text{Ni}(\text{dmit})_2]_2$ thin film. Also shown is a least-square fit (Gaussians), after a Shirley-type background subtraction, where each line (dashed) is composed of a spin–orbit split doublet with an energy separation E_{SO} and a branching ratio B . The addition of the three lines results in the continuous gray line. Results from the fit: $E(\text{C-S-Ni}) = 161.8 \text{ eV}$, $E(\text{C-S-C}) = 163.5 \text{ eV}$, $E(\text{C=S}) = 165.3 \text{ eV}$, $\Gamma = 1.5 \text{ eV}$, $E_{\text{SO}} = 1.1 \text{ eV}$ and $B = 0.5$.

on their relative intensities. In the nominal formula $\text{TTF}[\text{Ni}(\text{dmit})_2]_2$, there are 12 C–S–C, 8 C–S–Ni and 4 C=S bonds, which results in a ratio 3:2:1. From the fit the intensity ratio between the C–S–C and C–S–Ni contributions is 1.4, in excellent agreement with the nominal 1.5 value. For a molar ratio of TTF/Ni = 3 within the electrochemical solution, electron micrographs of a covered area show a dense film made of roughly spherical grains with sizes ranging from 0.6 to 1 μm (Fig. 23a). For a molar ratio of TTF/Ni = 0.75 and whatever the current density value, fibers are observed ($> 100 \mu\text{m}$ long and 1–5 μm width, Fig. 23b). Fig. 24 shows the infrared spectrum (absorbance vs. wavenumbers) of the electrodeposited material. It confirms the presence of both TTF and $\text{Ni}(\text{dmit})_2$ moieties within the films. The peak at $3081(\text{w}) \text{ cm}^{-1}$ corresponds to the CH ethylenic stretching vibrations for TTF. The band located at $509(\text{m}) \text{ cm}^{-1}$ corresponds to the symmetric stretching vibration of the two carbon–sulfur single bonds in the $\text{S}_2\text{C}=\text{S}$ fragment of dmit [43]. The characteristic doublet present in all compounds containing the $\text{M}(\text{dmit})_2$ moiety, displays maxima at $1051(\text{m})$ and $1071(\text{s}) \text{ cm}^{-1}$, respectively. The higher frequency peak of the doublet (1071 cm^{-1}) is assigned to the stretching vibration of carbon–sulfur double bond in the terminal $\text{S}_2\text{C}=\text{S}$ fragment of dmit, while the lower one (1051 cm^{-1}) corre-

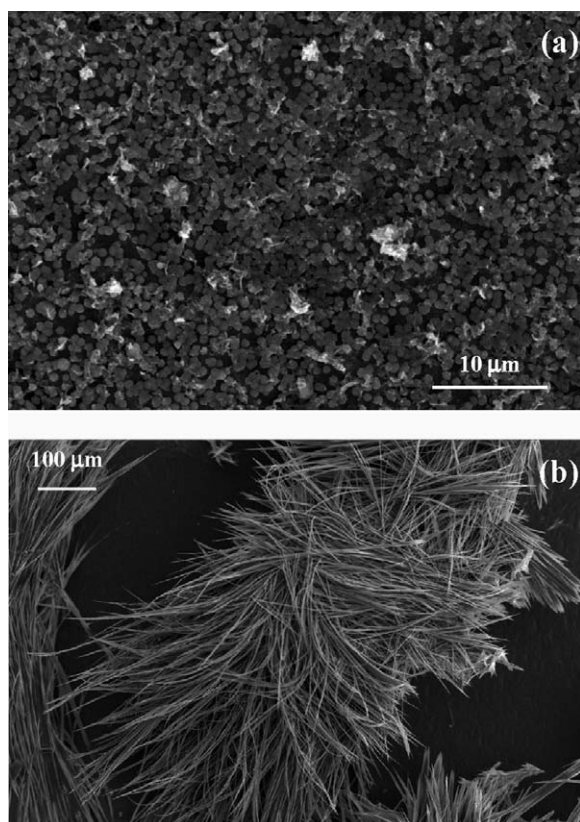


Fig. 23. SEM images of deposits of TTF[Ni(dmit)₂]₂ elaborated at 1.5 μA cm⁻² (a: TTF/Ni = 3; b: TTF/Ni = 0.75).

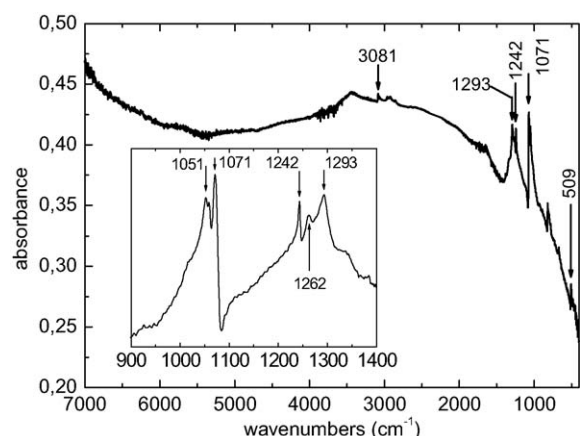


Fig. 24. Infrared spectrum of electrodeposited TTF[Ni(dmit)₂]₂ thin films.

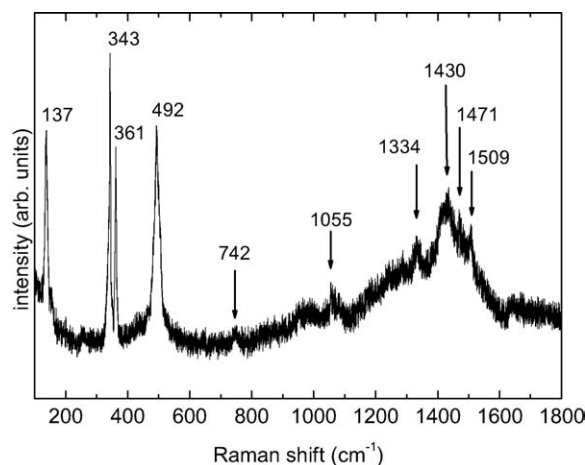


Fig. 25. Raman spectrum of electrodeposited TTF[Ni(dmit)₂]₂ thin films.

sponds to the Fermi resonance peak between overtones of symmetric stretching vibration of two carbon–sulfur single bonds in the S₂C=S fragment of dmit and the higher frequency [43]. For [N(*n*-C₄H₉)₄][Ni(dmit)₂], the doublet exhibits maxima at 1063 and 1030 cm⁻¹ [43]. The higher frequencies for the deposit confirm the less anionic character of the Ni(dmit)₂ skeleton. The Raman spectrum shown on Fig. 25 is in excellent agreement with that reported for TTF[Ni(dmit)₂]₂ single crystals [44]. Low-frequency bands are vibration modes related to the Ni(dmit)₂ entity: 137(s), 343(vs), 361(s), 492(s), and 1334(w) cm⁻¹ [39,45]. The C=C stretching modes at 1430(m), 1471(sh), and 1509(w) cm⁻¹ are related to the TTF moiety [46]. The lower frequency line (1430 cm⁻¹) involves a large contribution of the central carbon–carbon double bond in TTF (71%). This band, whose position is very sensitive to the amount of charge transfer (1518 cm⁻¹ for neutral TTF and 1420 cm⁻¹ for TTF⁺), allows us to determine a charge transfer of about 0.86 [47]. This value is in relatively good agreement with that obtained from band structure calculations, i.e. 0.80 [40]. The two other Raman lines at 1471 and 1509 cm⁻¹ are also lower compared to those for neutral TTF (1530 and 1555 cm⁻¹), confirming the cationic character of the TTF moiety. Fig. 26 shows the electrical behavior of the electrodeposited material: the ratio resistance at a given temperature (*T*) over resistance at 300 K [*R*(*T*)/*R*(300 K)] is reported as a function of the temperature. The samples exhibit a metallic behavior down to ca. 14 K, temperature at which the resistance slightly increases. At 14 K, the resistance is

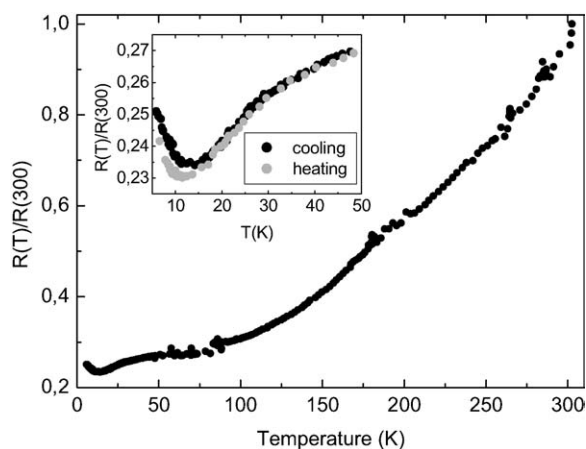


Fig. 26. Resistance as a function of temperature for electrodeposited TTF[Ni(dmit)₂]₂ thin films.

around 4.3 times smaller than the resistance at 300 K, and is still four times smaller at 4.5 K. Such a behavior is totally reversible, when warming back to room temperature. Such a reversibility has also been observed on single crystals of TTF[Ni(dmit)₂]₂ [48], but with a resistance at 4.4 K ~500 times smaller compared to the one at 300 K. Moreover the conductivity value is of ~12 S cm⁻¹ at room temperature, and larger than 50 S cm⁻¹ at 14 K.

4. General discussion

4.1. M(TCNE)_x magnets

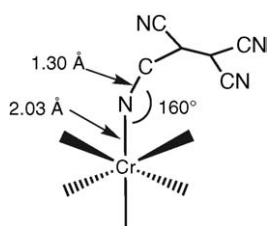
Previously to this work, we had reported the use of silicon wafers as substrates for growing TTF-based molecular semiconductors. During these studies, we have observed that [TTF][TCNQ] (TCNQ = tetracyanoquinodimethane) films appear as platelets (3 × 1 μm) and needles (diameter < 0.3 μm) [49], while [TTF-

(OH)TEMPO][TCNQ] (TEMPO = *N,N,N*-trimethyl-1-oxy-2,2,6,6-tetramethylpiperidin-4-yl) ones exhibit a micro-needle morphology (0.5–2 μm in length, 0.1–0.2 μm in diameter) [42]. Moreover, these films were found to be very adherent on the Si surface. The CVD-grown thin M(TCNE)_x magnets described in this paper exhibit a very different morphology. Whatever the metal nature, electron micrographs evidence continuous films showing more or less cracks (Figs. 1,6,12, and 15). However, these latter do not affect the adherence of the films onto the silicon surface. Thus, silicon is the substrate of choice due to its low weight over surface ratio, its wide use in the electronic domain and due to the fact that materials vapor deposited on it, keep their interesting magnetic properties.

All M(TCNE)_x deposits display a two-absorption peak pattern for ν_{CN} stretching modes (~2100 and ~2200 cm⁻¹, Table 3). Moreover, a shoulder in the range 2140–2180 cm⁻¹ is occasionally encountered. Therefore, it is concluded that TCNE is present as μ₂-, μ₃-, or μ₄-TCNE^{•-} [16]. It is also to be noticed that the complex and broad nature of the absorptions suggests that mixtures of bonding motifs are present. Furthermore, X-ray photoelectron surface analysis evidences both the presence of monoreduced TCNE (thus confirming infrared data), and the presence of the metal center in a low-oxidation state (typically, M^{II}). According to the literature, only M(TCNE)_x, y CH₂Cl₂ (M = Mn, Fe) magnets give X-ray powder patterns. However, they have never been indexed. M(TCNE)_x, y S are proposed to be composed of [TCNE^{•-}]_s being bound to up to four Ms most likely linearly, although some may be bent and each TCNE^{•-} is planar [16]. Because of the expected hexacoordination of M(II), each TCNE^{•-} may bind to three M(II)s, although some coordination sites may be occupied by solvent molecules [16]. The CVD-grown M(TCNE)_x phases described here show no diffraction line within the range $d = 7.5\text{--}3.5 \text{ \AA}$ (d : inter-reticular distance). We have explored the use of X-ray absorp-

Table 3
Summary of the ν_{CN} IR absorption data for vapor deposited M(TCNE)_x films

Compound	ν _{CN} (cm ⁻¹)
V(TCNE) _x (as-deposited)	2105(s), 2192(m)
V(TCNE) _x (after annealing)	2106(s), 2145(sh), 2195(m)
V(TCNE) _x (after annealing and 1 h air exposure)	No change compared to the above data
Cr(TCNE) _x	2116(s), 2202(m)
Nb(TCNE) _x	2102(s), 2180(sh), 2200(m)
Mo(TCNE) _x	2113(s), 2212(m)



Scheme 4. Basic model for the chromium environment in $\text{Cr}(\text{TCNE})_x$ magnets.

tion spectroscopy for structural investigations. Indeed, EXAFS has been widely used for studying Prussian blue-like materials [26]. For performing such an EXAFS study within the $\text{M}(\text{TCNE})_x$ series, the $\text{Cr}(\text{TCNE})_x$ phase, which displays a relatively large air stability, has been selected. The structural parameters are in agreement with an hexacoordination of $\text{Cr}(\text{II})$. The mean Cr-N distance is of 2.03 Å and the Cr-N-C angle is of about 160° (Scheme 4).

All $\text{M}(\text{TCNE})_x$ compounds prepared as thin films by CVD exhibit a spontaneous magnetization at low temperature (Table 4). As-deposited $\text{V}(\text{TCNE})_x$ exhibits a field-dependent magnetization between 5 and 300 K, and saturates to about 18 emuOe g^{-1} at 5 K and 800 Oe. Assuming $x \sim 2$ and a Landé factor of $g = 2$, this value is in good agreement with antiferromagnetic coupling between $S = 3/2 \text{ V}(\text{II})$ and two $S = 1/2 \text{ TCNE}^{\bullet-}$ species (i.e. $S_{\text{total}} = 1/2$) [18]. The saturation magnetization temperature dependence can be fit to the Bloch Law, $M_S = M_S(0) [1 - B T^{3/2}]$, of the spin wave theory [50], with $M_S(0) = 18.2 \text{ emuOe g}^{-1}$ and $B = 1.7 \times 10^{-4} \text{ K}^{-3/2}$. Using $B = 0.0587(k_B/2JS_{\text{total}})^{3/2}/S_{\text{total}}$, the average exchange energy, J/k_B , is 80 cm^{-1} . This value

is in rather good agreement with that reported for $\text{V}(\text{TCNE})_x$ magnets obtained by co-sublimation of $\text{V}(\text{CO})_6$ and TCNE (100 cm^{-1}) [22]. The hysteresis loop recorded at 300 K shows a coercive field of 80 Oe and a saturation magnetization of $\sim 2.5 \text{ emuOe g}^{-1}$ (Table 5). Thermal treatment (at 343 K for 10 h) reduces the magnetization by a factor of about 40 (Table 5). Further air exposure (1 h) does not destroy magnetic ordering at room temperature (Table 5). However, reduction in the magnetization value by a factor of about 5 is observed (with respect to the thermally treated sample kept under an argon atmosphere). The magnetic susceptibility of the $\text{Cr}(\text{TCNE})_x$ films has been measured between 2 and 300 K (Fig. 9). The temperature dependence of the susceptibility obeys the Curie–Weiss law above 80 K with a θ value of -95 K , a larger negative value than that observed for $\text{Cr}(\text{TCNE})_x$, $0.5 \text{ C}_6\text{H}_5\text{CH}_3$ prepared from $\text{Cr}(\text{naphthalene})_2$ and TCNE in toluene solution ($\theta = -75 \text{ K}$) [29]. Consequently, the magnetic interaction between the spin centers is strongly antiferromagnetic. Fig. 10 shows the hysteresis loop (magnetization versus applied magnetic field) at 2.5 K. The major feature in this data is the absence of saturation for fields up to 65 kOe. However, a coercive field of $\sim 100 \text{ Oe}$ at 2.5 K is clearly evidenced as shown in the insert in Fig. 10. We conclude that, at this temperature, magnetic ordering exists in the sample. At 2.5 K, the magnetization value for an applied field of 65 kOe is about 11 emuOe g^{-1} . Assuming a $\text{Cr}(\text{TCNE})_x \sim 2$ composition, an independent $S = 2, 1/2, 1/2$ system should have a saturation magnetization of $\sim 36 \text{ emuOe g}^{-1}$. Strong antiferromagnetic couplings, as evidenced by the large

Table 4
Magnetic data for vapor deposited $\text{M}(\text{TCNE})_x$ films at 5 K (V), 2.5 K (Cr, Nb), 2 K (Mo)

Compound	Saturation magnetization (emuOe g^{-1})	Saturation induction (Oe)	Coercive field (Oe)
$\text{V}(\text{TCNE})_x$ (as-deposited)	18 (a)	800	10
$\text{Cr}(\text{TCNE})_x$	11* (a)	–	100
$\text{Nb}(\text{TCNE})_x$	6×10^{-4} (b)	20,000	200
$\text{Mo}(\text{TCNE})_x$	0.5 (a)	50,000	20

* Magnetization value at 50,000 Oe, (a) per g of pure deposited material, (b) per g of substrate–film composite.

Table 5
Magnetic data for vapor deposited $\text{V}(\text{TCNE})_x$ films at 300 K

Compound	Saturation magnetization (emuOe g^{-1})	Saturation induction (Oe)	Coercive field (Oe)
$\text{V}(\text{TCNE})_x$ (as-deposited)	2.5	800	80
$\text{V}(\text{TCNE})_x$ (after annealing)	5.9×10^{-2}	2500	50
$\text{V}(\text{TCNE})_x$ (after annealing and 1 h exposure to air)	1.2×10^{-2}	1500	50

negative θ value, may explain the reduced magnetization values.

The $M(\text{TCNE})_{x,y}$ solvent complexes with a second-row transition metal have never been described before. The reaction of $\text{Nb}(\text{iPr}_2\text{-dad})_3$ in the presence of TCNE in refluxing toluene for 20 h leads to a low amount of black precipitate for which the results from the elemental analysis are not interpretable. Its infrared spectrum evidences a strong band at 2199 cm^{-1} assigned to coordinated TCNE and the characteristic vibration modes of the diazabutadiene ligands. Furthermore, the reaction of $\text{Nb}(\eta^6\text{-mes})_2$ (mes: mesitylene) in the presence of TCNE in toluene at room temperature leads instantaneously to a black precipitate. However, the solution is stirred at room temperature for a further 10 h to ensure total reaction. The precipitate is analyzed as $\text{Nb}(\text{TCNE})_{1.1} \cdot 0.4\text{ C}_7\text{H}_8$. Its infrared spectrum in the ν_{CN} region exhibits two broad absorptions at $2092(\text{s})$ and $2198(\text{s})\text{ cm}^{-1}$, in agreement with coordinated $\text{TCNE}^{\bullet-}$ species. Moreover, preliminary magnetic measurements evidence that the compound exhibits a spontaneous magnetization at 2 K (coercive field: 100 Oe). Therefore, $\text{Nb}(\eta^6\text{-mes})_2$ complex seemed to be the precursor of choice for growing thin films of $\text{Nb}(\text{TCNE})_x$ using the CVD technique. Although vaporization of the precursor was efficient, no deposit is obtained, at least in the explored conditions. $\text{Nb}(\text{TCNE})_x$ as thin film can be obtained from the $\text{Nb}(\text{iPr}_2\text{-dad})_3$ precursor (Table 1). Infrared spectra of the deposits display strong CN modes and small features corresponding to a low amount of diazabutadiene ligands remaining on the niobium atoms. The films exhibit a spontaneous magnetization at 2.5 K and a coercive field of ~ 200 Oe. Finally, $\text{Mo}(\text{TCNE})_x$ thin films obtained from the $\text{Mo}(\text{C}_6\text{H}_5\text{CH}_3)_2$ precursor (Table 1) also behave as permanent magnets at 2 K and display a coercive field of ~ 20 Oe.

As a conclusion to this section, we have shown the feasibility of producing thin films of $M(\text{TCNE})_x$ molecule-based magnets by CVD (M: first- or second-row transition metal, namely, V, Cr, Nb, Mo). There are found to be relatively adherent on the silicon surface and, by suppressing the deleterious effect of the solvent (observed on solution-grown $M(\text{TCNE})_{x,y}$ solvent compounds), they all exhibit a spontaneous magnetization (at low temperatures for Cr, Nb, and Mo, and in the temperature range 5–300 K for V).

4.2. Molecule-based conductors on Si

4.2.1. Non-integral oxidation state salt $[(n\text{-C}_4\text{H}_9)_4\text{N}]_2[\text{Ni}(\text{dcbdt})_2]_5$ as thin films

Thin films of $[(n\text{-C}_4\text{H}_9)_4\text{N}]_2[\text{Ni}(\text{dcbdt})_2]_5$ are obtained by electrolysis of a dichloromethane solution of $[(n\text{-C}_4\text{H}_9)_4\text{N}][\text{Ni}(\text{dcbdt})_2]$ on a silicon wafer used as anode (galvanostatic or potentiostatic conditions). Films mainly form on the non-polished face of the silicon electrode. Elemental analysis of a sample of film scratched from the surface gives the following results: %C = 49.90; %H = 2.77; %N = 11.05. These values are in good agreement with the data calculated for $[(n\text{-C}_4\text{H}_9)_4\text{N}]_2[\text{Ni}(\text{dcbdt})_2]_5$ (%C = 50.18; %H = 3.46; %N = 11.49). Therefore, the same 2:5 stoichiometry is obtained within the films. Under galvanostatic conditions, electron micrographs evidence that the film is made of thin platelets ($30\text{--}55\text{ }\mu\text{m}$ long, $1\text{--}8\text{ }\mu\text{m}$ width, thickness $< 1\text{ }\mu\text{m}$) randomly distributed on the substrate surface (Fig. 18a). This thin film morphology is in sharp contrast with the dendritic growth reported for $[(n\text{-C}_4\text{H}_9)_4\text{N}]_{0.9}[\text{Ni}(\text{dmid})_2]$ on a Pt metal foil [7] and also for $[(n\text{-C}_4\text{H}_9)_4\text{N}]_2[\text{Ni}(\text{dcbdt})_2]_5$ platelets on platinum wires [14], both at high current densities (i.e. $25\text{ }\mu\text{A cm}^{-2}$). As a matter of fact, in our case, much lower current densities ($0.5\text{ }\mu\text{A cm}^{-2}$) are applied and could favor the growth of long platelets or needles. A SEM side view of a segment of the film peeled off from the surface allows us to evaluate the thickness at $\sim 10\text{ }\mu\text{m}$. As expected, under potentiostatic conditions ($E_{\text{app}} = 1.0\text{ V vs. SCE}$), that is at higher growth rates than in galvanostatic conditions, the quantity of material appears much higher. Moreover, the quality of micro-crystals is also lower (Fig. 18b). The electrical conductivity of $[(n\text{-C}_4\text{H}_9)_4\text{N}]_2[\text{Ni}(\text{dcbdt})_2]_5$ thin films (elaborated under galvanostatic conditions) is about $1.2 \times 10^{-2}\text{ S cm}^{-1}$ at room temperature and follows a thermally activated semiconducting behavior. The plot of $\log(\sigma)$ versus $1/T$ shows an activation energy of 157 meV in the range 295–230 K (Fig. 21). This value is reduced to 67 meV below 230 K. A similar semiconducting behavior was observed on single crystals with very similar activation energy values (176 meV at high temperatures and 68 meV below 250 K) [37]. The origin of this noticeable change in the activation energy is not yet clear and may be associated to a phase transition. The room temperature conductivity of the film is one order of magnitude lower than that of single crys-

tals (0.15 S cm^{-1}). The $[-210]$ direction, which is the stacking direction and the direction of highest conductivity, also corresponds to the direction of the long axis of the needle-like crystals [37]. As electron micrographs show that the grown needles lay on the surface, the direction of highest conductivity is part of the plane in which the film conductivity is measured. This feature, the contributions of other directions within the crystallites, and the polycrystalline nature of the film, which generates grain boundaries, account for the lower conductivity value of the film versus that of the crystal. However, the conductivity ratio between single crystal and film is rather low and indicative of a more than one-dimensional system.

4.2.2. Charge transfer salt $\text{TTF}[\text{Ni}(\text{dmit})_2]_2$ as thin films

Deposits of $\text{TTF}[\text{Ni}(\text{dmit})_2]_2$ are obtained by electrolysis of an acetonitrile solution of TTF and $[(n\text{-C}_4\text{H}_9)_4\text{N}][\text{Ni}(\text{dmit})_2]$ on a silicon wafer used as anode (galvanostatic conditions, see Table 2). Deposits form on both the polish and the non-polished faces of the silicon electrode. They are adherent and insensitive towards an air exposure. When a molar ratio $\text{TTF}/\text{Ni} = 3$ is used (at $1.5 \mu\text{A cm}^{-2}$), a dense film made of roughly spherical grains (size: $0.6\text{--}1 \mu\text{m}$) is observed (Fig. 23a). About 15% of the surface remains non-covered. To evaluate the thickness of the films, side views of the sample were difficult to perform. However, assuming a 'monolayer' of grains (as observed on SEM), a thickness of the order of magnitude of $1 \mu\text{m}$ seems reasonable. When a molar ratio $\text{TTF}/\text{Ni} = 0.75$ is used (at $0.8, 1.5,$ or $2.5 \mu\text{A cm}^{-2}$), simple eye observation shows that the silicon surface is poorly covered. Within the covered areas, electron micrographs evidence the presence of severely aggregated micro-fibers (several hundred micrometers long, $1\text{--}5 \mu\text{m}$ wide, Fig. 23b). For higher current densities (1.5 and $2.5 \mu\text{A cm}^{-2}$), these fibers have a certain tendency to be aligned. However, the effect of stoichiometry on morphology and surface covering is not yet understood. Electrodeposited $\text{TTF}[\text{Ni}(\text{dmit})_2]_2$ thin films (elaborated at $1.5 \mu\text{A cm}^{-2}$ with excess TTF) have a metallic behavior down to ca. 14 K , temperature at which the resistance slightly increases. Moreover, this behavior is totally reversible, when warming back to room temperature, as previously observed on $\text{TTF}[\text{Ni}(\text{dmit})_2]_2$ as single crystals [48]. Taking into account the size and

shape of the studied sample, this leads to a conductivity of ca. 12 S cm^{-1} at room temperature, and larger than 50 S cm^{-1} at 14 K . Obviously, these values are much lower than the values reported for the conductivities on single crystals (300 S cm^{-1} at 300 K , and $1.5 \times 10^5 \text{ S cm}^{-1}$ at 2 K) [48]. Nevertheless, it should be pointed out here that, whatever the substrate, the conductivity of thin films is usually very low, as observed for $[\text{TTF}][\text{TCNQ}]$ (0.4 S cm^{-1}) [49], or $(\text{BEDT-TTF})(\text{ClO}_4)_x$ ($10^{-3} \text{ S cm}^{-1}$) [51]. Moreover, these thin films usually exhibit a semiconducting behavior, due in part to grain boundaries and/or heterogeneous morphologies. However, transparent composite films made of polycarbonate/ θ - $(\text{BET-TTF})_2\text{Br} \cdot 3 \text{ H}_2\text{O}$ have been recently described and showed metal-like transport properties down to liquid helium temperature, with $\sigma_{\text{RT}} \sim 100 \text{ S cm}^{-1}$ [52]. Nevertheless, it is worth noting that our films are, to our knowledge, the first example with a dithiolate complex, displaying a metallic behavior down to very low temperature.

5. Conclusion

We have shown the feasibility of producing thin films of molecule-based magnets by CVD, and thin films of molecule-based conductors by electrodeposition. We have explored the use of silicon substrates, whose importance in the electronic domain is obvious. $\text{M}(\text{TCNE})_x$ magnets are grown from the gas phase reaction of an organometallic complex and TCNE. These materials present potential magnetic shielding and inductive applications [53,54]. Thin films of two molecule-based conductors, namely $[(n\text{-C}_4\text{H}_9)_4\text{N}]_2[\text{Ni}(\text{dcbdt})_2]_5$, and $\text{TTF}[\text{Ni}(\text{dmit})_2]_2$ have been processed by using the electrodeposition technique. $\text{TTF}[\text{Ni}(\text{dmit})_2]_2$ as thin films exhibits a well-defined metallic behavior down to about 14 K . The metallic behavior evidences that low inter-grain conduction energy barriers are achieved, in contrast with most thin films of highly-conducting materials reported to date. Since $\text{TTF}[\text{Ni}(\text{dmit})_2]_2$ undergoes a superconducting transition (critical temperature: 1.6 K under 7 kbar hydrostatic pressure), our results open the possibility of preparing superconducting thin films of other molecule-based materials, in spite of their polycrystalline morphology, based on the well-known and extensively-used electrodeposition technique.

Acknowledgements

H. Casellas thanks the French government for funding her Ph.D. by a MENESR grant. J.-P. Savy thanks the Fond Social Européen (FSE) for a grant. The authors gratefully thank Dr. F. Villain for X-ray absorption spectra, Dr. A. Zwick for Raman measurements, Dr. F. Senocq for XRD data, Dr. J. Fraxedas for X-ray photoelectron spectra, Dr. A. Mari for magnetic measurements, Professor M. Almeida for supplying the $[(n\text{-C}_4\text{H}_9)_4\text{N}][\text{Ni}(\text{dcbdt})_2]$ starting complex, and V. Collière for SEM micrographs. D. Bérail from Motorola is acknowledged for supplying supports for conductivity measurements.

References

- [1] J. Fraxedas, *Adv. Mater.* 14 (2002) 1603.
- [2] S. Nakanishi, G. Lu, H.M. Kothari, E.W. Bohannon, J.A. Switzer, *J. Am. Chem. Soc.* 125 (2003) 14998.
- [3] W.E. Buschmann, S.C. Paulson, C.W. Wynn, M.A. Girtu, A.J. Epstein, H.S. White, S. Miller, *Chem. Mater.* 10 (1998) 1386.
- [4] O. Sato, T. Iyoda, A. Fujishima, K. Hashimoto, *Science* 271 (1996) 49.
- [5] G.R. Torres, B. Agricole, P. Delhaes, C. Mingotaud, *Chem. Mater.* 14 (2002) 4012.
- [6] T. Takahashi, K.-i. Sakai, T. Yumoto, T. Akutagawa, T. Hasegawa, T. Nakamura, *Thin Solid Films* 393 (2001) 7.
- [7] S.G. Liu, P.J. Wu, Y.Q. Liu, D.B. Zhu, *Mol. Cryst. Liq. Cryst.* 275 (1996) 211.
- [8] H. Isotalo, J. Paloheimo, Y.F. Miura, R. Azumi, M. Matsumoto, T. Nakamura, *Phys. Rev. B* 51 (1995) 1809.
- [9] E.O. Fischer, *Inorg. Synth.* 6 (1960) 132.
- [10] P.J. Daff, M. Etienne, B. Donnadiou, S.Z. Knottenbelt, J.E. McGrady, *J. Am. Chem. Soc.* 124 (2002) 3818.
- [11] G. Pampaloni, F. Calderazzo, L. Rocchi, *J. Organomet. Chem.* 413 (1991) 91.
- [12] M.L.H. Green, W.E. Silverthorn, *J. Chem. Soc., Dalton Trans.* (1973) 301.
- [13] G. Steimecke, H.-J. Sieler, R. Kirmse, E. Hoyer, *Phosphorus Sulfur* 7 (1979) 49.
- [14] D. Simão, H. Alves, D. Belo, S. Rabaça, E.B. Lopes, I.C. Santos, V. Gama, M.T. Duarte, R.T. Henriques, H. Novais, M. Almeida, *Eur. J. Inorg. Chem.* 12 (2001) 3119.
- [15] D. de Caro, J. Sakah, M. Basso-Bert, C. Faulmann, J.-P. Legros, T. Ondarçuhu, C. Joachim, L. Ariès, L. Valade, P. Cassoux, *C. R. Acad. Sci. Paris, Ser. IIc* 3 (2000) 675.
- [16] J.S. Miller, *Inorg. Chem.* 39 (2000) 4392.
- [17] S. Ferlay, T. Mallah, R. Ouahès, P. Veillet, M. Verdaguer, *Nature* 378 (1995) 701.
- [18] J.S. Miller, A.J. Epstein, *J. Chem. Soc. Chem. Commun.* 13 (1998) 1319.
- [19] D. de Caro, M. Basso-Bert, J. Sakah, H. Casellas, J.-P. Legros, L. Valade, P. Cassoux, *Chem. Mater.* 12 (2000) 587.
- [20] H. Casellas, D. de Caro, L. Valade, P. Cassoux, *Chem. Vap. Deposition* 8 (2002) 145.
- [21] K.-I. Sugiura, S. Mikami, K. Iwasaki, S. Hino, E. Asato, Y. Sakata, *J. Mater. Chem.* 10 (2000) 315.
- [22] K.I. Pokhodnya, A.J. Epstein, J.S. Miller, *Adv. Mater.* 12 (2000) 410.
- [23] X. He, M. Trudeau, D. Antonelli, *Inorg. Chem.* 40 (2001) 6463.
- [24] D.T. Clark, D.B. Adams, *Chem. Phys. Lett.* 10 (1971) 121.
- [25] V. Briois, P. Lagarde, C. Brouder, P. Sainctavit, M. Verdaguer, *Physica B* 208 (1995) 51 & 209.
- [26] R. Garde, F. Villain, M. Verdaguer, *J. Am. Chem. Soc.* 124 (2002) 10531.
- [27] S.I. Zabinsky, J.J. Rehr, J.J. Ankudinov, R.C. Albers, M.J. Eller, *Phys. Rev. B* 52 (1995) 2995.
- [28] A.G. Orpen, L. Brammer, F.H. Allen, O. Kennard, D.G. Watson, R. Taylor, *J. Chem. Soc., Dalton Trans.* 12 (1989) S1–S83.
- [29] D.C. Gordon, L. Deakin, A.M. Arif, J.S. Miller, *J. Am. Chem. Soc.* 122 (2000) 290.
- [30] N.K. Huang, B. Tsuchiya, K. Neubeck, S. Yamamoto, K. Narumi, Y. Aoki, H. Abe, A. Miyashita, H. Ohno, H. Naramoto, *Nucl. Instr. Meth. Phys. Res. B* 143 (1998) 479.
- [31] D. Briggs, M.P. Seah, *Practical Surface Analysis*, vol. 1, second ed., Wiley, New York, 1990.
- [32] S.O. Grim, L.J. Matienzo, *Inorg. Chem.* 14 (1975) 1014.
- [33] K.-i. Sugiura, S. Mikami, K. Iwasaki, S. Hino, E. Asato, Y. Sakata, *J. Mater. Chem.* 10 (2000) 315.
- [34] R. Gross-Lannert, W. Kaim, B. Olbrich-Deussner, *Inorg. Chem.* 29 (1990) 5046.
- [35] C. Faulmann, P. Cassoux, in: E.I. Stiefel (Ed.), *Dithiolene Chemistry, Synthesis, Properties, and Applications*, Wiley, Hoboken, 2004, p. 399.
- [36] H. Alves, D. Simão, I.C. Santos, V. Gama, R.T. Henriques, H. Novais, M. Almeida, *Eur. J. Inorg. Chem.* 6 (2004) 1318.
- [37] H. Alves, I.C. Santos, E.B. Lopes, D. Belo, V. Gama, D. Simão, H. Novais, M.T. Duarte, R.T. Henriques, M. Almeida, *Synth. Met.* 133 (2003) 397.
- [38] H.L. Liu, D.B. Tanner, A.E. Pullen, K.A. Abboud, J.R. Reynolds, *Phys. Rev. B* 53 (1996) 10557.
- [39] K.I. Pokhodnya, C. Faulmann, I. Malfant, R. Andreu-Solano, P. Cassoux, A. Mlayah, D. Smirnov, J. Leotin, *Synth. Met.* 103 (1999) 2016.
- [40] P. Cassoux, L. Valade, in: D.W. Bruce, D. O'Hare (Eds.), *Inorganic Materials*, Wiley, Chichester, 1996, p. 1.
- [41] L. Brossard, M. Ribault, M. Bousseau, L. Valade, P. Cassoux, *C.R. Acad. Sci. Paris, Ser. II* 302 (1986) 205.

- [42] H. Casellas, D. de Caro, L. Valade, J. Fraxedas, *New J. Chem.* 26 (2002) 915.
- [43] G. Liu, Q. Fang, W. Xu, H. Chen, C. Wang, *Spectrochim. Acta [A]* 60 (2004) 541.
- [44] L. Valade, H. Casellas, S. Roques, C. Faulmann, D. de Caro, A. Zwick, L. Ariès, *J. Solid-State Chem.* 168 (2002) 438.
- [45] R. Ramakumar, Y. Tanaka, K. Yamaji, *Phys. Rev. B* 53 (1996) 10557.
- [46] R. Bozio, I. Zanon, A. Giraldo, C. Pecile, *J. Chem. Phys.* 71 (1979) 2282.
- [47] A.R. Siedle, in: J.S. Miller (Ed.), *Extended Linear Chain Compounds*, vol. 2, Plenum Press, New York, 1982, p. 469.
- [48] M. Bousseau, L. Valade, J.-P. Legros, P. Cassoux, M. Garbauskas, L.V. Interrante, *J. Am. Chem. Soc.* 108 (1986) 1908.
- [49] S. Caillieux, D. de Caro, L. Valade, M. Basso-Bert, C. Faulmann, I. Malfant, H. Casellas, L. Ouahab, J. Fraxedas, A. Zwick, *J. Mater. Chem.* 13 (2003) 2931.
- [50] C. Kittel, *Introduction to Solid State Physics*, Wiley, New York, 1976.
- [51] Y.F. Miura, G.E.M. Tovar, S. Ohnishi, M. Hara, H. Sasabe, W. Knoll, *Thin Solid Films* 393 (2001) 225.
- [52] M. Mas-Torrent, E. Laukhina, C. Rovira, J. Veciana, V. Tkacheva, L. Zorina, S. Khasanov, *Adv. Funct. Mater.* 11 (2001) 299.
- [53] J.M. Manriquez, G.T. Yee, R.S. McLean, A.J. Epstein, J.S. Miller, *Science* 252 (1991) 1415.
- [54] B.G. Morin, C. Hahn, J.S. Miller, A.J. Epstein, *J. Appl. Phys.* 75 (1994) 5782.